WIND TUNNEL INVESTIGATION OF SUPERSONIC WING-TAIL FLUTTER

Lawrence J. Huttsell, Thomas E. Noll
and Donald E. Holsapple

Air Force Flight Dynamics Laboratory

SUMMARY

An experimental and analytical study was undertaken to establish the flutter trends of a highly swept wing-tail configuration in the low supersonic speed regime. Wind tunnel flutter data was also required for evaluating a new supersonic aerodynamic method for predicting wing-tail interference. A flutter model, consisting of a wing, horizontal tail, and splitter plate/fuselage mechanism, was tested in the Arnold Engineering Development Center (AEDC) Propulsion Wind Tunnel Facility (PWT) 4-Foot Transonic Tunnel in the Mach number range 1.1 to 1.3. Two types of flutter were encountered during the testing; a wing-tail flutter mode and a tail bending-torsion flutter mode. The wing-tail flutter speed was found to be a minimum at M = 1.2 for the configuration tested. Recorded model test data were digitized for a power spectral density (PSD) analysis and Random Decrement (Randomdec) analysis. Comparisons between the frequency and damping obtained from the PSD plots and the Randomdec signatures agreed very well. A limited flutter analysis was conducted using a Mach box unsteady aerodynamics method which accounted for interference and airfoil thickness. Analytical comparisons with experimental flutter speeds agreed very well. The analyses assuming zero thickness predicted flutter speeds higher than those measured, ranging from 1 percent at M = 1.12 to 8 percent at M = 1.28. With the airfoil thickness included, the correlation was improved such that predicted flutter speeds for all cases investigated were within 2 percent of experimental speeds. Flutter frequencies were not as well predicted, generally being somewhat higher than measured.

SYMBOLS

b	wing semichord measured streamwise and intersecting the elastic axis line at 75-percent wing span
f	frequency
g	structural damping coefficient
m	wing mass per unit span
M	freestream Mach number
P_T	total pressure

V freestream velocity at flutter

ρ air density

μ model to air mass ratio, $\frac{m}{\pi\rho b^2}$

ω flutter frequency

ω_h wing first coupled cantilever bending frequency

ω_θ uncoupled fuselage torsion frequency

INTRODUCTION

Today's advanced military aircraft must be capable of undertaking multi-mission roles. Variable sweep wings are used on some aircraft configurations for improving performance at different flight conditions. Low wing sweep angles are attractive during takeoff, landing, and long range cruise when higher aspect ratio is required; high wing sweep angles, which reduce drag, are desirable for high speed flight.

Initially it was thought that flutter speeds would increase at the high sweep angles thus complementing the use of the variable sweep wing. However, in 1966, Topp, Rowe, and Shattuck (Reference 1) conducted a theoretical and experimental program which determined that there are cases where this does not occur. Model tests indicated that for low sweep angles, the critical flutter mode involved the high frequency bending-torsion motion of the wing. As expected, the flutter speed increased as the wing was initially swept back. Near 58 degrees wing sweep, however, a new flutter mode involving the lower frequency modes of the wing, fuselage, and tail became evident. With further increases in wing sweep, the flutter speed dropped rapidly, and at 70 degrees, the flutter speed was lower than for the most forward swept case. The cause for the lower flutter speed and its rapid drop with increasing wing sweep was not fully understood at this time. Since this was a new unforeseen phenomenon, not predictable using available aerodynamic theories, further theoretical and experimental studies were conducted in the following years.

One of the first experimental programs in the area following the effort by Topp, et al., was sponsored by the Air Force Flight Dynamics Laboratory (AFFDL). In 1966, Balcerak (Reference 2) designed, constructed, and tested a series of constant chord 45 degree and 60 degree swept wing-horizontal tail flutter models. Wing and tail surfaces were identical in planform. Testing was accomplished at Mach numbers ranging from 0.4 to 1.24 and defined the effects of important wing-tail parameters on flutter. In some cases the flutter speed continued to decrease into the low supersonic speed regime.

In 1968, the AFFDL continued their investigation by conducting subsonic wind tunnel tests and analyses on a semispan model of a representative variable sweep wing aircraft configuration (Reference 3). Similar trends of flutter

speed versus sweep angle were found. The AFFDL paralleled the experimental investigation with a detailed theoretical study. Both a doublet-lattice method (Reference 4) and a kernal function method (References 5 and 6) were employed to predict the aerodynamic interaction between the wing and tail. Both methods predicted the flutter frequencies extremely well. Flutter speeds were conservatively predicted ranging up to 20 percent lower than the measured flutter velocities. Also, the theory predicted the flutter speed to decrease with increasing subsonic Mach number.

Since the transonic tests of Reference 2 showed that flutter speeds decreased as the Mach number increased, at least up to Mach 1.24, the development of a method to predict unsteady aerodynamic loads for interfering surfaces was required for the supersonic speed regime. Under AFFDL sponsorship, a Mach box method (References 7 and 8) was developed for supersonic interfering surfaces. This paper describes supersonic flutter tests of a half-span flutter model which was dynamically scaled from the model used in the earlier subsonic effort (Reference 3), and the limited analyses which were conducted for verifying the Mach box aerodynamic method.

SUPERSONIC WING-TAIL FLUTTER MODEL

The Air Force Flight Dynamics Laboratory defined the general design of a half-span flutter model consisting of a wing, horizontal tail, and splitter plate/fuselage mechanism. The detail design and construction of the model was performed by Atkins and Merrill, Inc., Ashland, Massachusetts.

The supersonic model was designed to flutter within the Arnold Engineering Development Center (AEDC) PWT 4-Foot Transonic Wind Tunnel by dynamically scaling the 60 degree sweep subsonic model of Reference 3, with the exception of the horizontal tail. The design fundamental frequency for the supersonic tail model was twice that of the wing. Higher tail frequencies were not obtained because the high stiffness characteristics of the subsonic tail could not practically be scaled due to the very low mass requirements for the supersonic model.

Figure 1 provides a photograph of the model showing the wing and tail surfaces, the splitter plate/fuselage mechanism, and the tunnel mounting system. The fuselage mechanism and the wing and tail attachments were enclosed within the fairing between the splitter plate and tunnel ceiling. The model was mounted from the tunnel ceiling in such a manner as to simulate antisymmetric vibration modes. This was achieved by attaching the models to a shaft assembly which was supported by bearings, thereby providing a roll degree of freedom. A roll stiffness was provided by a small spring mounted between the shaft assembly and the splitter plate. Variation in the fuselage torsional stiffness was obtained by changing the effective length of a constant cross-sectional bar which connected the fore and aft shaft assemblies. The wing and tail could either roll together or differentially since the shaft assemblies for the wing and tail surfaces were interconnected only through the torsion bar. Variations in the torsion bar length could be accomplished without affecting the separation

between the wing and tail. Two tail attachment points were also provided to allow a variation in horizontal separation between the wing and tail.

The wing and tail models were constructed using a stressed skin fabrication technique. This composite construction consisted of laminated fiberglass/epoxy skins which were high-temperature cured under pressure and stabilized with a honeycomb core. Strips of graphite were added along the span of the wing and tail to obtain the required bending stiffness. The wing was attached to the forward fuselage roll bar by means of a flexible carry-through structure with scaled torsion and bending stiffnesses. The tail was attached to the aft fuselage roll assembly by means of a carry-through structure with high stiffness.

Natural mode shapes and frequencies were computed using classical lumped mass methods. Figure 2 shows typical results for four elastic modes used in the flutter analysis. In general, agreement between the wing measured and predicted node lines and frequencies was good. The first mode (not shown in the figure) involves roll motion about the model roll axis with a measured frequency of 17.8 Hz; the second mode involves primarily wing carry-through torsion coupled with wing bending; the third mode involves tail bending and wing bending; the fourth mode involves primarily wing second bending and carry-through torsion; and the fifth mode is primarily tail torsion.

WIND TUNNEL TESTS

The tests were conducted in the AEDC PWT 4-Foot Transonic Wind Tunnel. A schematic of the data monitoring and recording system used during the flutter tests is shown in Figure 3. During testing, strain gage bridges were used to monitor and record the response of the model. Strain gage bridges were mounted just outboard of the wing and tail roots to measure the bending and torsion strains. Others were mounted on springs to measure wing carry-through torsion and bending, the fuselage torsion, and the model roll motions. The eight strain gage channels and a time code were displayed on a Varian strip recorder and copied on tape together with a voice track. Two X-Y oscilloscopes were used to monitor the coupling of the critical wing-tail modes; one of the oscilloscopes displayed fuselage torsion (FT) and wing carry-through torsion (CT) responses; the second oscilloscope displayed wing carry-through bending (CB) and wing carry-through torsion (CT) responses. An on-line Time/Data analyzer was used to display the frequency response (0-100 Hz) for either the wing carry-through torsion, the wing carry-through bending, or the fuselage torsion motion. The approximate frequency range of high model response was determined from such a display. Modes of interest were selected and processed through a 5 Hz bandwidth tracking filter to define the critical frequency.

The test Mach number was approached from a low total pressure (low dynamic pressure). The total pressure was increased at an essentially constant Mach number until flutter occurred. At selected test conditions, the response data was recorded and the frequencies measured using the tracking filter. Figure 4 presents the AEDC 4T wind tunnel standard operating envelope of total pressure

and dynamic pressure versus Mach number, and shows the flutter points obtained for each configuration tested. The first test configuration, wing bending to fuselage torsion frequency ratio (ω_h/ω_θ) of 0.62, was tested at M = 1.2 up to a total pressure of 129.3 kPa (2700 psf). No flutter was encountered. However, there was significant wing and tail motion, indicating the proximity to flutter. The structural damping coefficient (g) was estimated to be approximately 0.01. Tunnel limitations prevented further testing of this configuration. The fuselage torsional stiffness was then adjusted to give ω_h/ω_θ = 0.32, and the model was again tested. Wing-tail flutter was obtained at M = 1.12, 1.2, and 1.28. The flutter frequency varied from 85 Hz at M = 1.12 to 88 Hz at M = 1.28. Figure 5 presents a strip chart recording for the M = 1.28 test configuration. Both wing and tail responses are shown to be diverging, indicating that the test condition was slightly into an unstable region. The flutter mode resulted in catastropic damage to both surfaces as shown in Figure 6.

A tail bending-torsion flutter mode was encountered at M = 1.08 while reducing Mach number at a constant total pressure from the M = 1.12 wing-tail flutter point. The frequency of the tail flutter mode was 176 Hz which is slightly above the tail torsion mode shown in Figure 2. The time history response record for the wing and tail strain gages are shown in Figure 7 for this mode of flutter. The tail bending and torsion gages diverged very rapidly. The motion on the wing is very small in comparison to the tail motions for this predominantly tail bending-torsion coupling. The tail surface was rapidly destroyed following flutter onset.

DATA REDUCTION

Following the wind tunnel tests, selected flutter model response data were played back from analog tapes and digitized using an ITI 4900-Preston A/D system. Low pass analog filters (48 dB per octave roll-off) were used to band limit the digitized response data to a frequency range of 0-200 Hz. Both Power Spectral Density (PSD) and Random Decrement (Randomdec) analyses methods were used to reduce the test data.

PSD Method

Narrow band (0.46 Hz bandwidth) PSD analyses were performed using a Raytheon 704 Fast Fourier Analyzer system. Thirteen transforms with sample size of 2048 were averaged to provide a spectrum which was plotted on the Raytheon/Gould 4800 plotter. Figures 8 and 9 present the results of the PSD analysis of the random response data for the model with ω_h/ω_θ = 0.32 and M = 1.2 at two subcritical test conditions (total pressures of 95.8 kPa (2000 psf) and 105.3 kPa (2200 psf)). The response in the 84-86 Hz mode (the critical wing-tail mode) increased with total pressure as flutter was approached. At a total pressure of 105.3 kPa (2200 psf), the response in a 176 Hz mode became more evident. The frequency and damping were estimated from the PSD plots using standard techniques, and the results are presented in Table I for the critical wing-tail mode at the two test conditions discussed above and at two additional points.

Randomdec Method

The Randomdec method, invented by H. A. Cole, Jr. (References 9 and 10) was applied in this study to analyze the response generated by random excitation for determining the frequency and damping of the modes of interest. The Randomdec program used ensemble averaging of up to 300 digital samples of response data (.07 seconds in length). The program extracted the characteristic response signature, and the frequency and damping ratio from the random response data (0-200 Hz). A typical Randomdec signature for $\omega_h/\omega_\theta = 0.32$ is shown in Figure 10 for M = 1.2 and P_T = 2000 psf. This corresponds to the PSD plot shown in Figure 8. The Randomdec signature is very clean, and the structural damping can be easily determined.

Comparison of Results Using PSD and Randomdec Methods

The structural damping coefficient and frequency for the critical wing-tail mode which were obtained using PSD and Randomdec methods are presented in Table I. All frequency comparisons are within 2 percent. Structural damping comparisons between the two methods are within 0.012. At a total pressure of 110.1 kPa (2300 psf), flutter onset has been slightly exceeded as shown by a small negative damping whereas the PSD method is not capable of providing negative damping.

ANALYSIS AND CORRELATION

Limited flutter analyses were conducted using the supersonic Mach box program described in References 7 and 8. This method was developed to analyze lifting surfaces in close proximity in supersonic flow including aerodynamic interference. The analyses were conducted for the flight conditions at which wing-tail flutter occurred for $\omega_h/\omega_\theta = 0.32$. These analyses were conducted both with and without airfoil thickness included. The Mach box method includes an option for thickness corrections to the pressure distribution based on second order piston theory.

Table II presents comparisons of calculated flutter speeds and frequencies with corresponding measured values at Mach numbers 1.12, 1.2 and 1.28. Without airfoil thickness included, the analyses predicted flutter speeds ranging from approximately 1 percent at M = 1.12 to 8 percent higher than the measured speeds at M = 1.28. With the airfoil thickness included in the analyses, flutter speed predictions were improved. At M = 1.2, the calculated flutter speed was within 1.5 percent of the measured flutter speed, a 5 percent improvement over the analyses without airfoil thickness. At M = 1.28, the analyses with airfoil thickness included was within 1 percent of the measured flutter speed, an improvement of approximately 7 percent. Flutter frequencies were not as well predicted. The calculated flutter frequencies were 8 to 18 percent higher than the measured values.

Both measured and calculated flutter data are presented in Figures 11 and 12 in the form of flutter parameters $V/b\omega_\theta \sqrt{\mu}$ and ω/ω_θ versus Mach number.

The subsonic data from Reference 3 are also shown for comparison. In Figure 11, the predicted subsonic trend of $V/b\omega_\theta \sqrt{\mu}$ is decreasing with Mach number as shown for $\omega_h/\omega_\theta = 0.62$. The trend for $\omega_h/\omega_\theta = 0.32$ is shown dashed, since analyses were not conducted for the configuration but were estimated based on other similar trends. These subsonic analyses indicate that $V/b\omega_\theta \sqrt{\mu}$ continues to drop at least up to transonic speeds. The supersonic test results for $\omega_h/\omega_\theta = 0.32$ indicate that a minimum flutter speed was obtained at M = 1.2. This was significantly lower than the M = 0 subsonic test results. A further increase in Mach number to M = 1.28 provided some alleviation; however, the flutter parameter still remains below the M = 0 test results. The supersonic analyses, with or without airfoil thickness included, show increasing flutter speeds with increasing Mach number.

Figure 12 presents ω/ω_θ versus Mach number. Test results indicate an increasing value of ω/ω_θ as the Mach number increases, while the analyses predict a minimum flutter frequency ratio at approximately M = 1.2 followed by an increase at the higher Mach number tested (M = 1.28).

CONCLUDING REMARKS

In conclusion, the results of this wind tunnel investigation of a wing-tail flutter phenomena in the Mach number range 1.12 to 1.28 show less stability (lower flutter speed parameter) than earlier corresponding subsonic data. However, the results indicate some increase in flutter stability at M = 1.28 as compared with M = 1.2 data. Also, the Mach box analysis procedure with aerodynamic interference and airfoil thickness effects included was found to adequately predict the wing-tail flutter speeds of this phenomena.

REFERENCES

1. Topp, L.J., Rowe, W.S., and Shattuck, A.W.: Aeroelastic Considerations in the Design of Variable Sweep Airplanes. ICAS Paper 66-12, Fifth International Congress of the Aeronautical Sciences, London, England, September 1966.

2. Balcerak, J.C.: Flutter Tests of Variable Sweep Configurations. AFFDL-TR-68-101, September 1968.

3. Mykytow, W.J., Noll, T.E., Huttsell, L.J., and Shirk, M.H.: Subsonic Flutter Characteristics of a Variable Sweep Wing and Horizontal Tail Combination. AFFDL-TR-69-59, November 1970.

4. Albano, E. and Rodden, W.P.: A Doublet Lattice Method for Calculating Lift Distributions on Oscillating Surfaces in Subsonic Flows. AIAA Journal, Vol. 7, No. 2, February 1969, pages 279-285.

5. Laschka, B. and Schmid, H.: Unsteady Aerodynamic Forces on Coplanar Lifting Surfaces in Subsonic Flow (Wing-Horizontal Tail Interference). Presented at AGARD Structures and Materials Panel Meeting, Ottawa, Canada, September 1967.

6. Albano, E., Perkinson, F., and Rodden, W.P.: Subsonic Lifting Surface Theory Aerodynamics and Flutter Analysis of Interfering Wing/Horizontal Tail Configurations. AFFDL-TR-70-59, September 1970.

7. Ii, J.M., Borland, C.J., and Hogley, J.R.: Prediction of Unsteady Aerodynamic Loadings of Non-Planar Wings and Wing-Tail Configurations in Supersonic Flow, Part I, "Theoretical Development, Program Usage, and Application". AFFDL-TR-71-108, March 1972.

8. Kramer, G.D. and Keylon, G.E.: Prediction of Unsteady Aerodynamic Loadings of Non-Planar Wings and Wing-Tail Configurations in Supersonic Flow, Part II, "Computer Program Description". AFFDL-TR-71-108, March 1972.

9. Cole, H.A., Jr.: Method and Apparatus for Measuring Damping Characteristics of a Structure. United States Patent No. 3, 620, 069, 16 November 1971.

10. Cole, H.A., Jr.: On-Line Failure Detection and Damping Measurement of Aerospace Structures by Random Decrement Signatures. NASA CR-2205, March 1973.

Table I. - Damping Comparison for the Critical Wing-Tail Mode at M = 1.2, $\omega_h/\omega_\theta = 0.32$.

P_T (kPa)	PSD f (Hz)	PSD g	RANDOMDEC f (Hz)	RANDOMDEC g
95.76	84.0	0.100	85.2	0.096
100.55	86.0	0.070	85.6	0.058
105.34	86.5	0.020	87.0	0.009
110.12	86.1	-	87.0	-0.009

Table II. - Airfoil Thickness Effects on Flutter Trends, $\omega_h/\omega_\theta = 0.32$.

MACH NUMBER	ANALYSIS ZERO THICKNESS V_{CAL}/V_{EXP}	ANALYSIS ZERO THICKNESS $\omega_{CAL}/\omega_{EXP}$	ANALYSIS THICKNESS (NACA 64-006) V_{CAL}/V_{EXP}	ANALYSIS THICKNESS (NACA 64-006) $\omega_{CAL}/\omega_{EXP}$
1.12	1.013	1.167	-	-
1.20	1.064	1.081	1.015	1.128
1.28	1.077	1.182	0.993	1.136

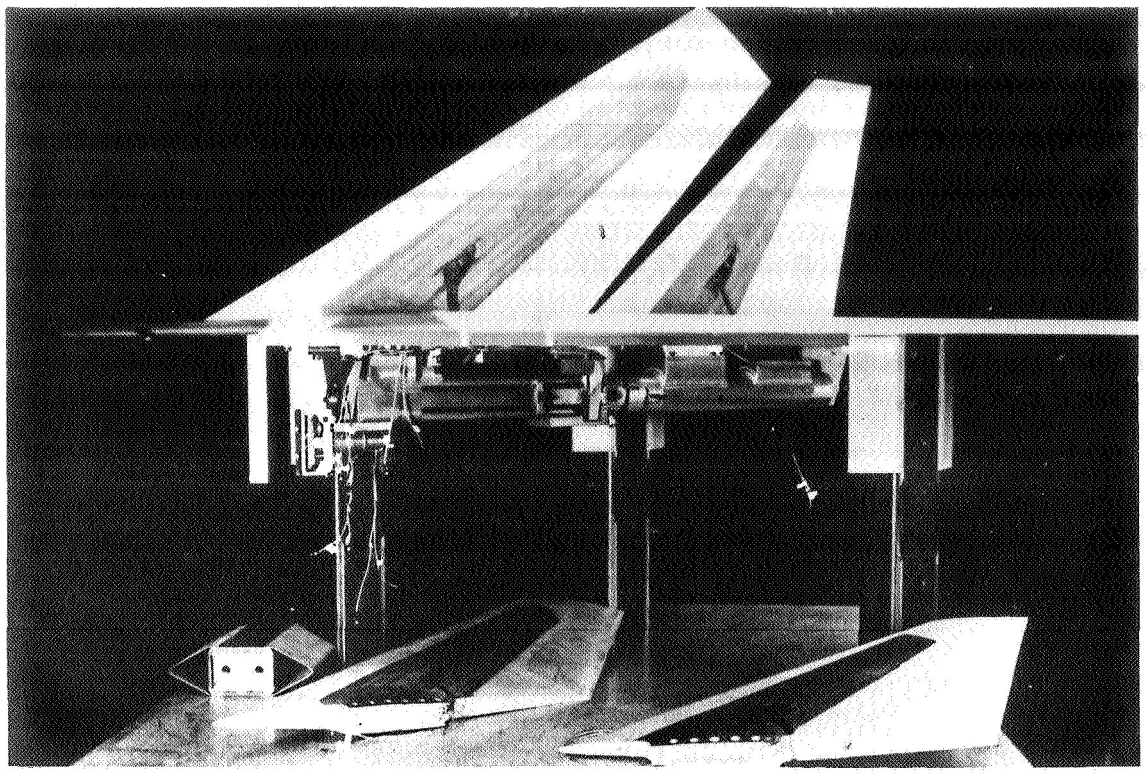

Figure 1. - Supersonic Wing-Tail Flutter Model.

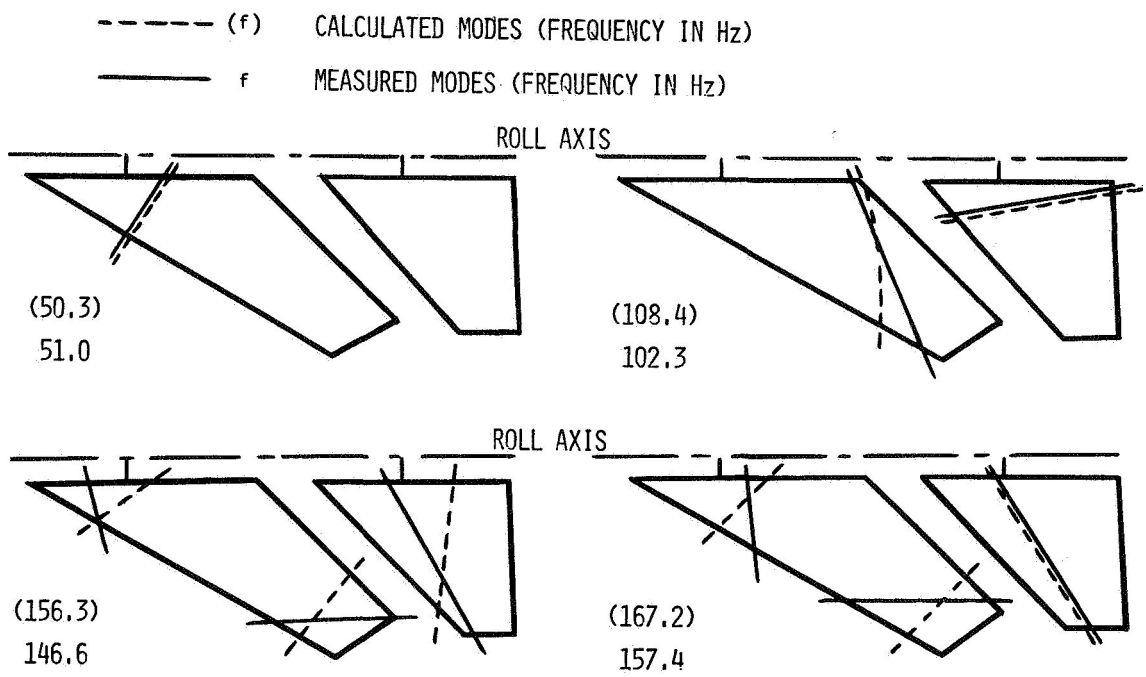

Figure 2. - Calculated and Measured Vibration Node Lines and Frequencies, $\omega_h/\omega_\theta = 0.32$.

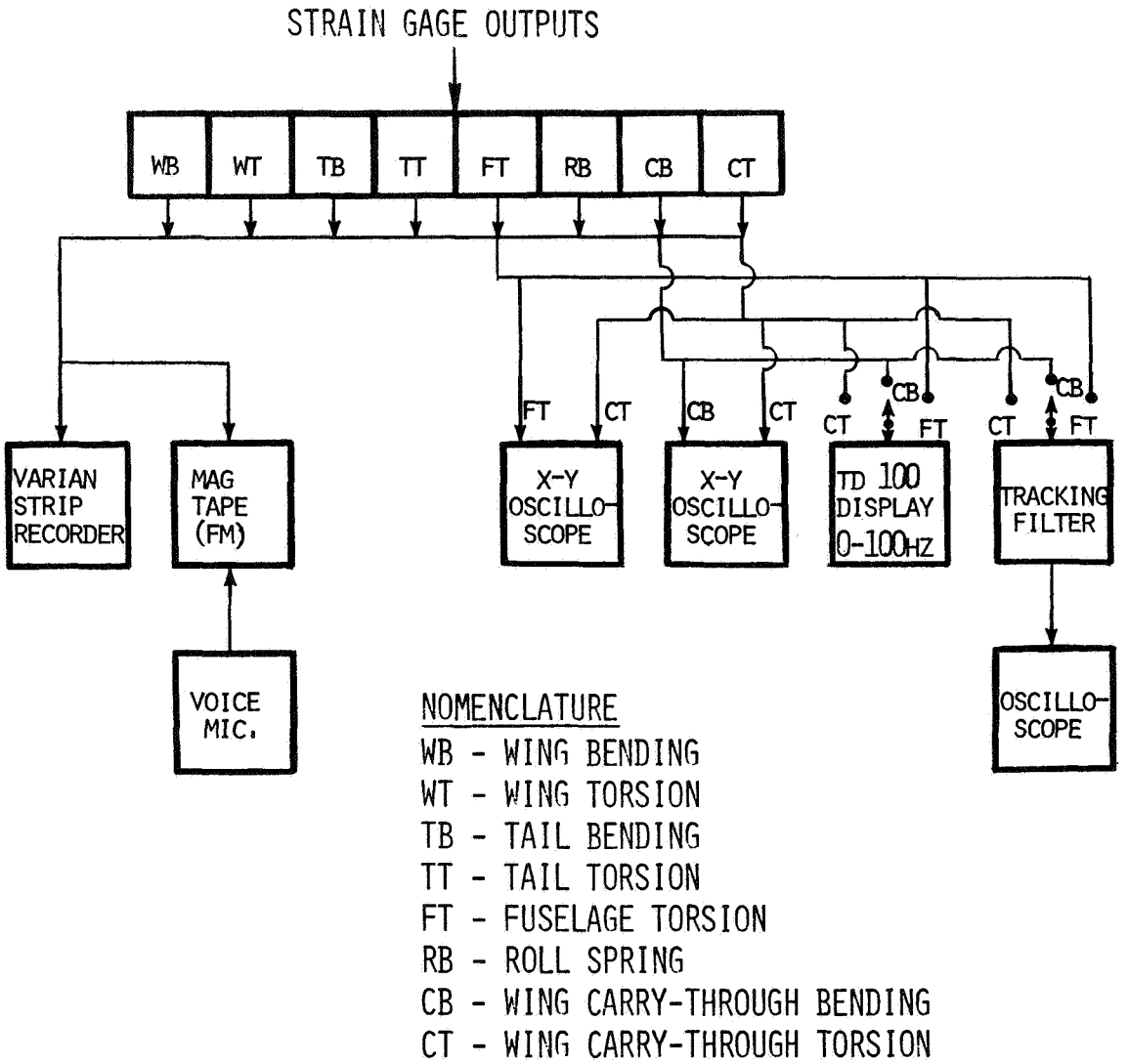

Figure 3. - Wind Tunnel Test Data Monitoring and Recording System.

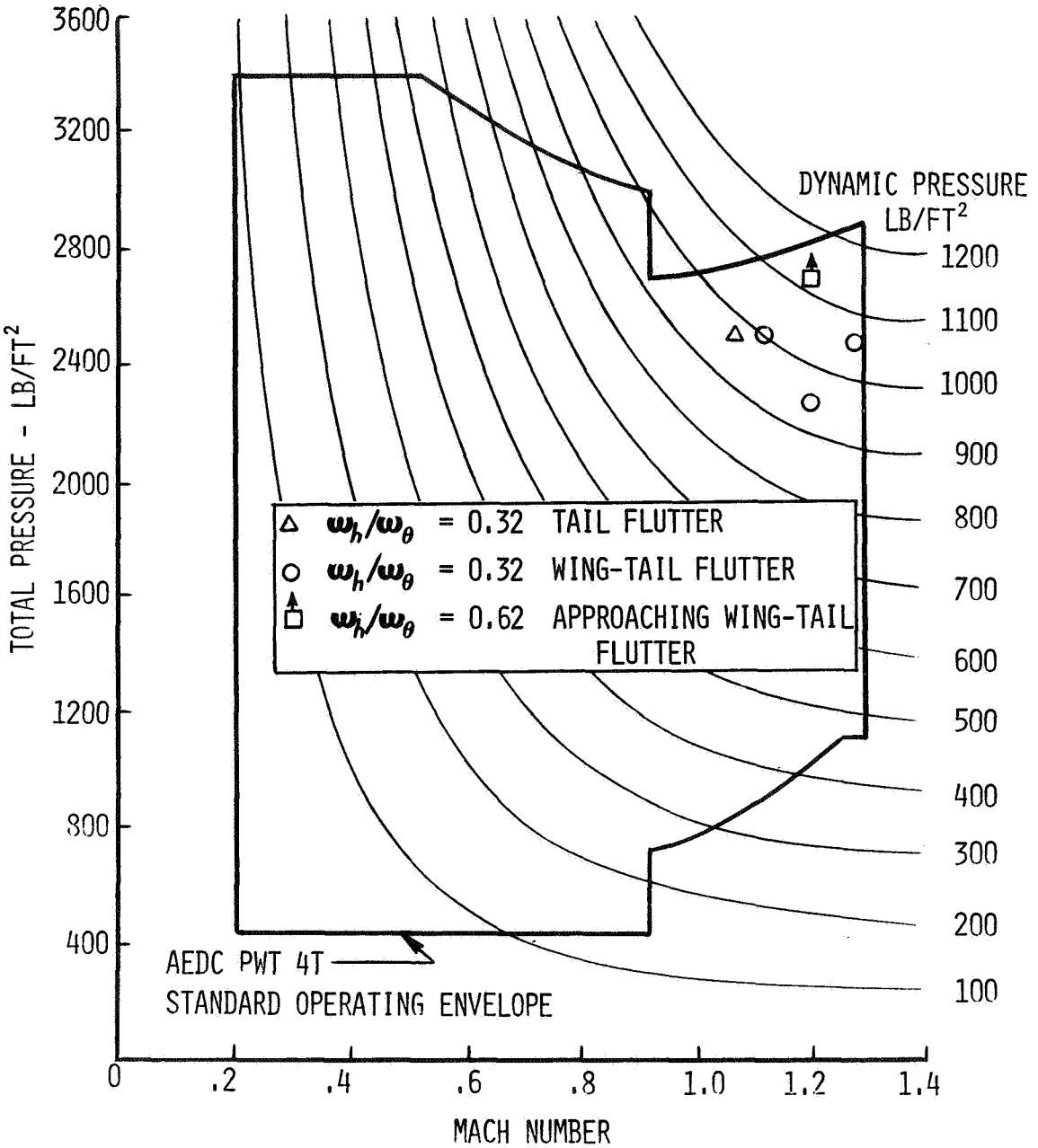

Figure 4. Wind Tunnel Operating Envelope with Experimental Flutter Data. (1 lb/ft^2 = 47.88 Pa.)

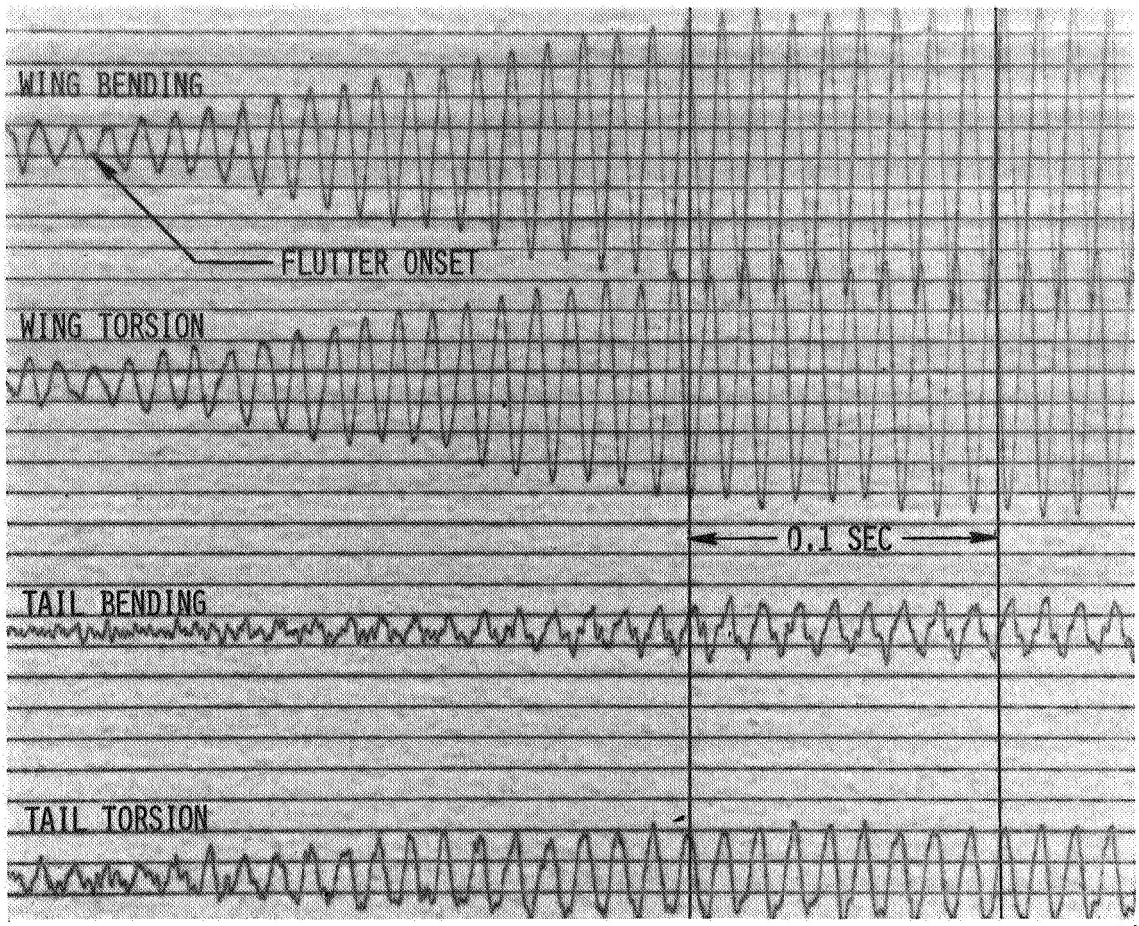

Figure 5. - Model Response at M = 1.28 and P_T = 118.5 kPa (2475 lb/ft^2), ω_h/ω_θ = 0.32.

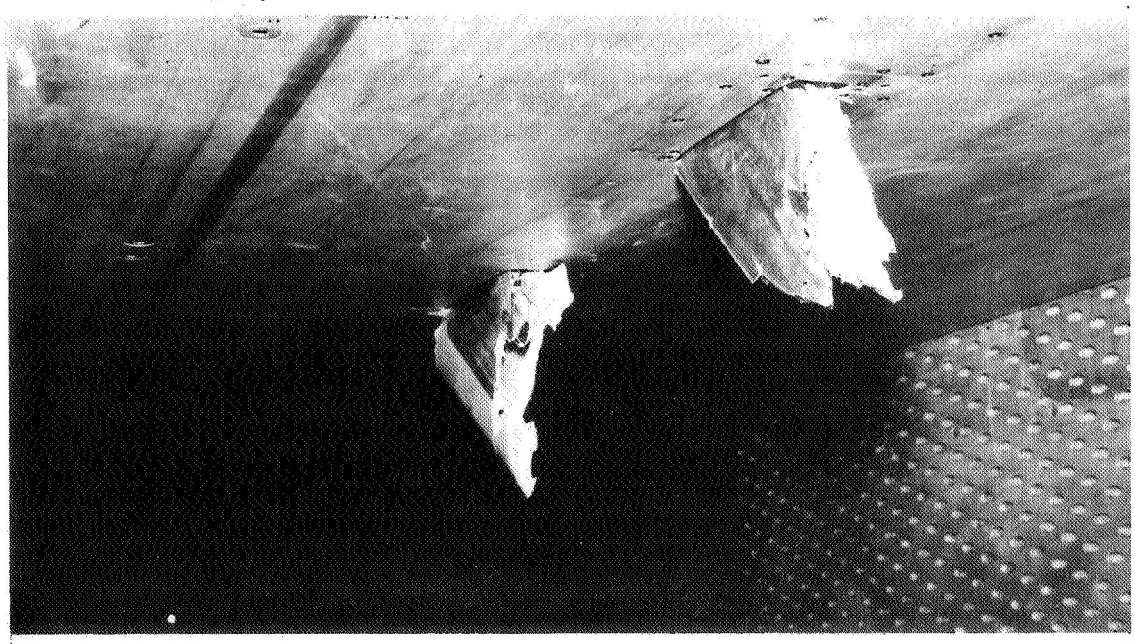

Figure 6. - Model Damage from Wing-Tail Flutter at M = 1.28, ω_h/ω_θ = 0.32.

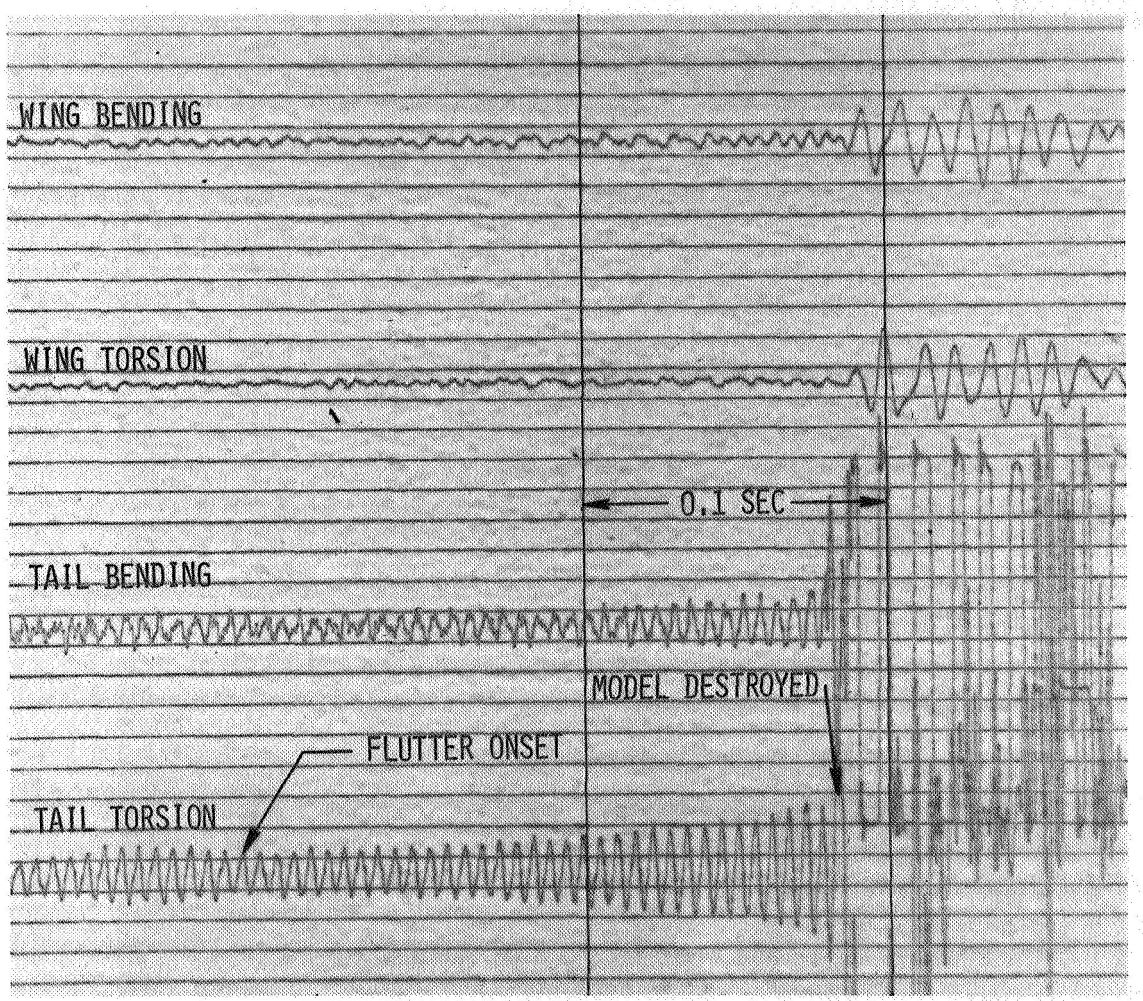

Figure 7. - Model Response at M = 1.08 and P_T = 119.7 kPa (2500 lb/ft^2), ω_h/ω_θ = 0.32.

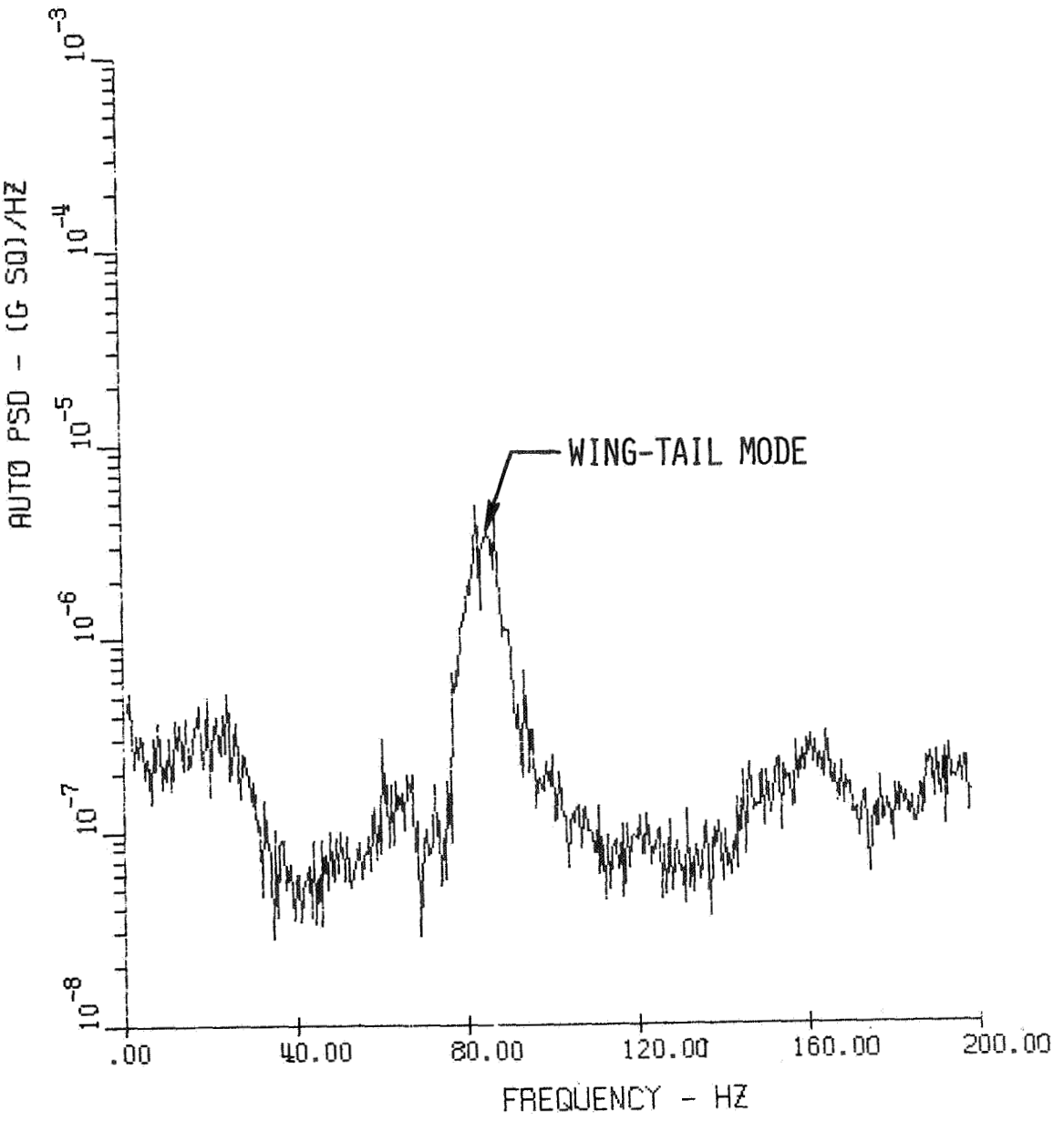

Figure 8. - PSD Plot for M = 1.2 and P_T = 95.8 kPa (2000 lb/ft^2), ω_h/ω_θ = 0.32.

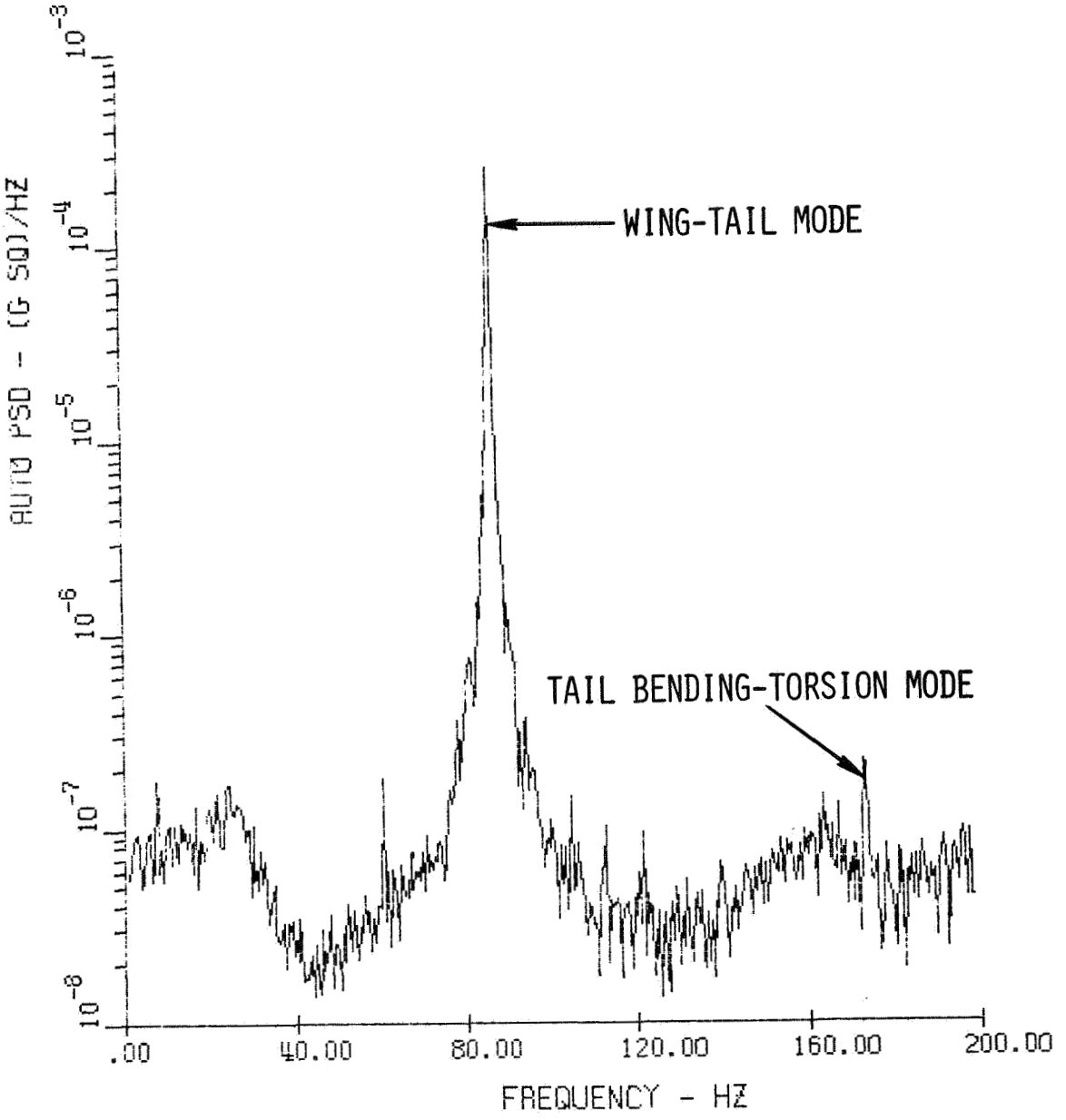

Figure 9. - PSD Plot for M = 1.2 and P_T = 105.3 kPa (2200 lb/ft^2), ω_h/ω_θ = 0.32.

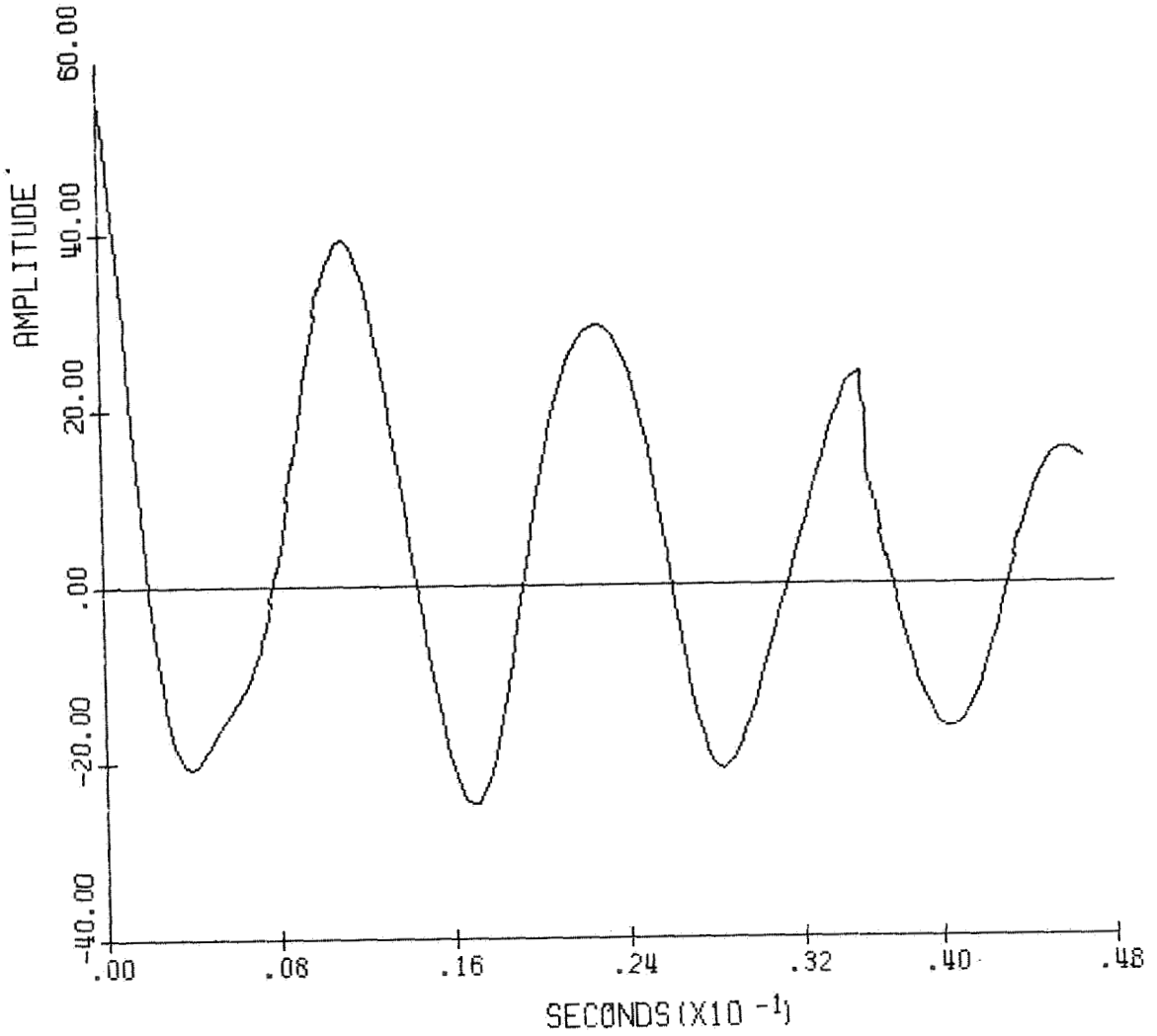

Figure 10. - Randomdec Signature for M = 1.2 and P_T = 95.8 kPa (2000 lb/ft^2), ω_h/ω_θ = 0.32.

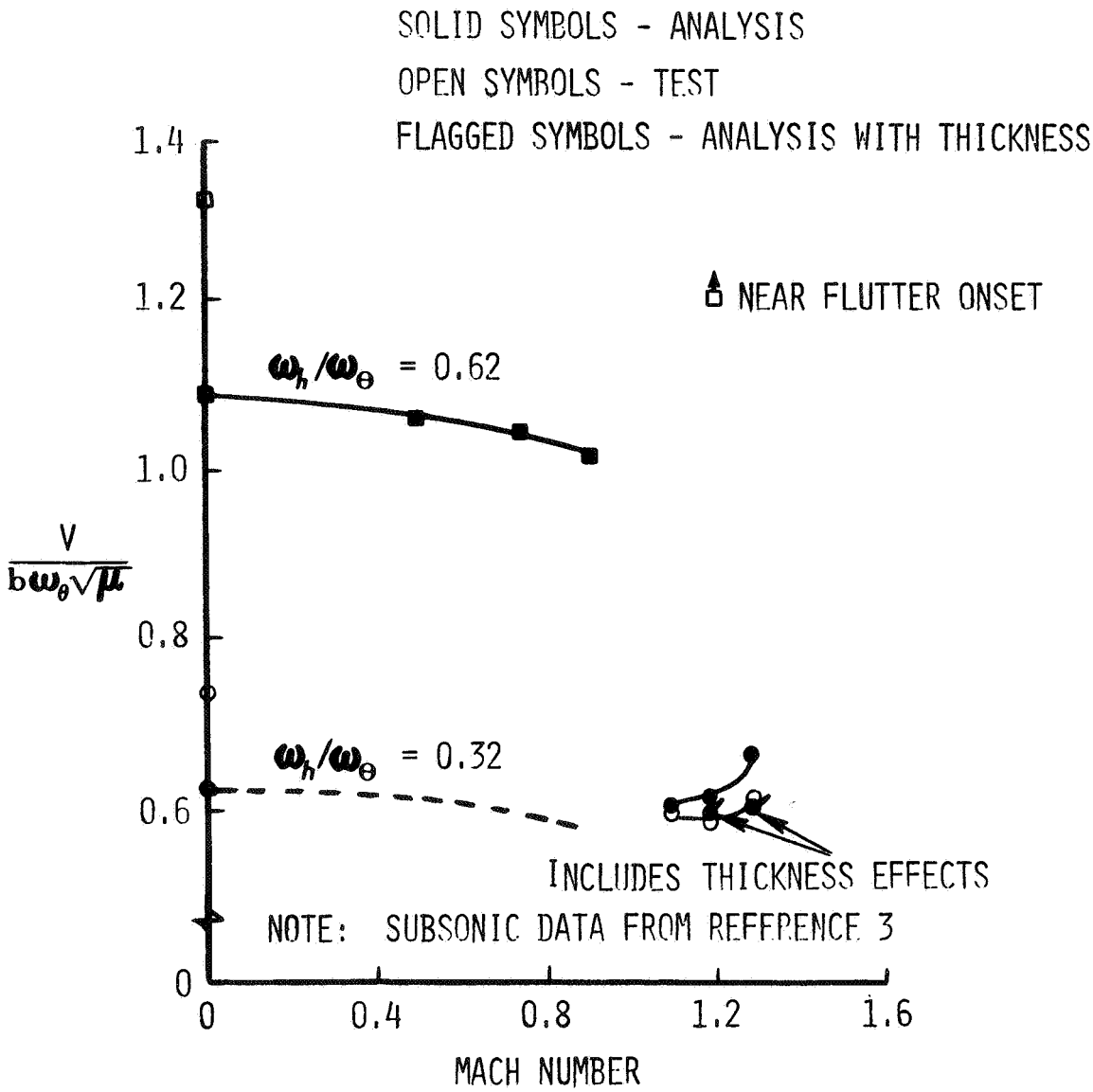

Figure 11. - $V/b\omega_\theta\sqrt{\mu}$ Versus Mach Number.

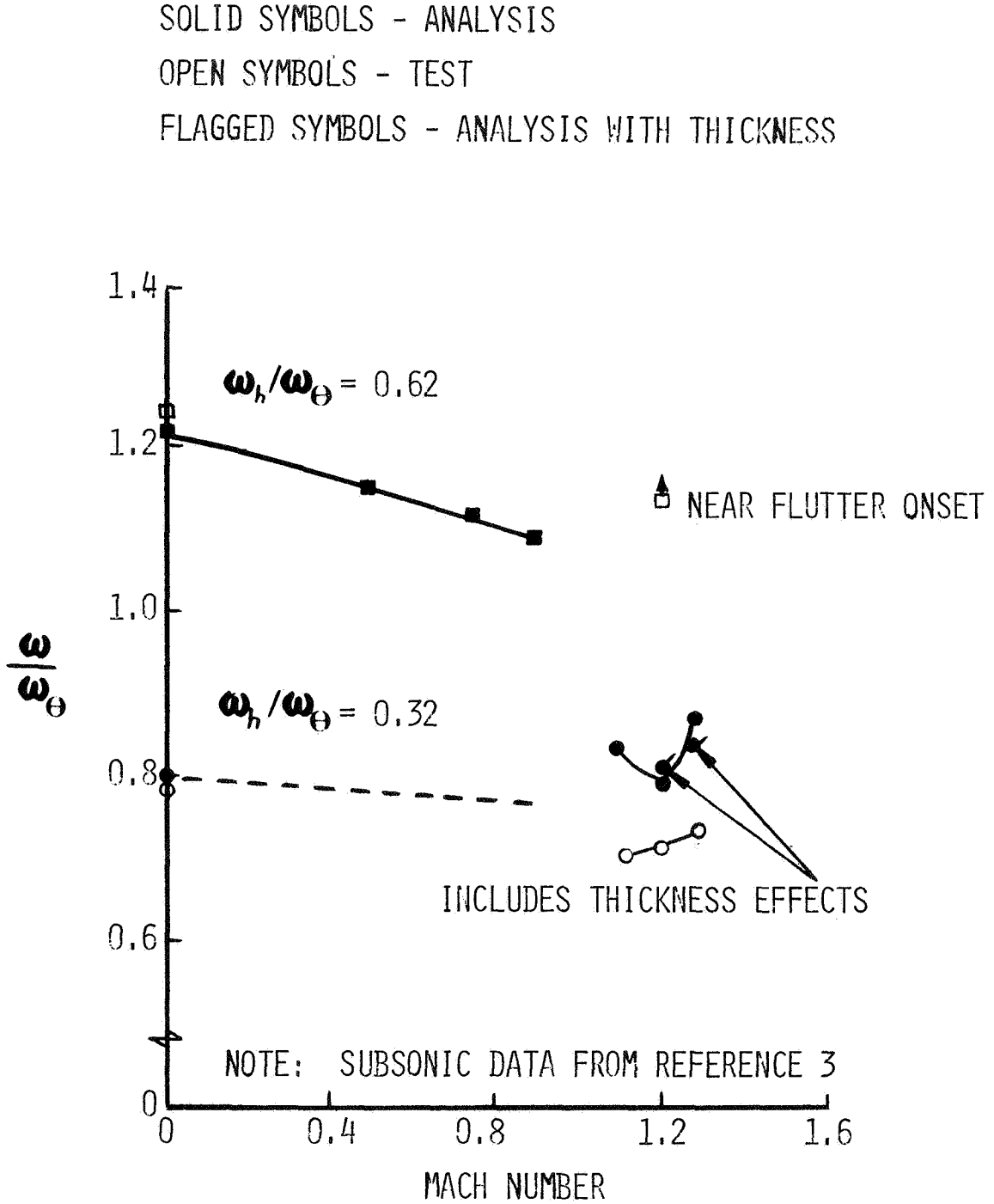

Figure 12. - ω/ω_θ Versus Mach Number.